PHYSICAL REVIEW B VOLUME 17, NUMBER 6 15 MARCH 1978

Pseudopotential calculations for $(GaAs)_1$-$(AlAs)_1$ and related monolayer heterostructures

Ed Caruthers* and P. J. Lin-Chung
Naval Research Laboratory, Washington, D. C. 20375
(Received 18 November 1977)

New atomic pseudopotential form factors are found for Ga, Al, and As. These simultaneously fit the energy bands of pure GaAs and AlAs. With these, eigenvalues and eigenvectors of the $(GaAs)_1$-$(AlAs)_1$ monolayer heterostructure are found and the density of states, the dielectric functions, and the charge density are calculated. With the additional assumption of the virtual-crystal approximation, the composition dependence of the principal valence-band maxima and conduction-band minima is found for $Ga_{1-x}Al_xAs$, $(Ga_{1-x}Al_xAs)_1$-$(Al_{1-x}Ga_xAs)_1$, and $(GaAs)_1$-$(Ga_{1-x}Al_xAs)_1$. It is shown that $(GaAs)_1$-$(AlAs)_1$ has electronic properties which are quite distinct from GaAs, AlAs, and $Ga_{0.5}Al_{0.5}As$. The effects of disorder on the principal band gaps are discussed. The theoretical results are compared to past experiments and several new experiments are suggested.

I. INTRODUCTION

Molecular-beam epitaxy (MBE) is capable of great precision in preparing GaAs-$Ga_{1-x}Al_xAs$ heterostructures.[1,2] These materials are characterized by the alternation of thin layers of the two kinds of semiconductor along the heterostructure axis. Molecular-beam epitaxy produces layers of uniform thickness over areas >2–3 mm^2. Disorder at interfaces between planes is believed to be confined to about one atomic layer.[3] In principle, therefore, it should be possible to fabricate monolayer heterostructures, i.e., heterostructures in which single atomic layers of Ga, As, Al, and As repeat in the zinc-blende (ZB) [001] direction. Gossard and co-workers have, in fact, recently reported achieving several thin-layer heterostructures $(GaAs)_m-(AlAs)_n$, $1 \leq n$, $m \leq 10$, where m and n denote numbers of atomic layers.[4] Experimental measurements indicate that the $m \approx n \approx 1$ materials so far produced contain about 30% disorder.[5] This disorder is described as "islandlike"; that is, individual layers are believed to be uniformly thick, but, e.g., a layer nominally denoted GaAs would actually contain ~30% AlAs clustered in almost pure islands. Experimental measurements must therefore be made on materials whose exact structure and composition may be known only approximately. In view of this, it seems desirable to have theoretically calculated properties of the perfect $(GaAs)_1$-$(AlAs)_1$ structure and of some related monolayer heterostructure for comparison with experimental results. We have performed a semiempirical pseudopotential calculation on $(GaAs)_1$-$(AlAs)_1$ and found detailed energy bands, the density of states, the dielectric functions, and the valence charge density. As reported earlier,[6] the lowest band gap for this material is direct, approximately 0.51 eV narrower than the $Ga_{0.5}Al_{0.5}As$ indirect band gap, and very difficult to observe by optical techniques. With the assumption that the virtual-crystal approximation[7] (VCA) can be used to treat substitutional alloys $Ga_{1-x}Al_xAs$, we have calculated the composition dependence of the principal conduction-band minima and valence-band maxima for the $(Ga_{1-x}Al_xAs)_1$ – $(Al_{1-x}Ga_xAs)_1$ and $(GaAs)_1$-$(Ga_{1-x}Al_xAs)_1$ monolayer heterostructures. As we shall see, the VCA can be used successfully for $Ga_{1-x}Al_xAs$ though it fails for other alloys. Its success lies in the perfect match of the lattice constants and dielectric constants between GaAs and AlAs.

The presentation of our results is as follows. In Sec. II we describe the $(GaAs)_1$-$(AlAs)_1$ crystal structure and our computational methods. In Sec. III we present detailed results for the $(GaAs)_1$-$(AlAs)_1$ electronic structure. In Sec. IV we justify our use of the VCA, present results for the alloy heterostructures mentioned above, and compare our results to experiment. Finally, in Sec. V, we summarize our results and offer some suggestions for experimental work to test these results.

II. CRYSTAL STRUCTURES AND COMPUTATIONAL METHODS

Figure 1(a) shows the unit cell for the ideal monolayer heterostructure. In this figure the atomic planes are stacked in the z direction and the coordinate axes are chosen to be along the cube edges of the pure GaAs fcc cell. Figure 1(b) shows this structure viewed from along the z axis. The dashed lines indicate the boundaries of the unit cell. The lattice constants for GaAs and AlAs are 5.64 Å and 5.63 Å, respectively. Because of this lattice constant matching, thick-layer heterostructures can be formed without a high density of mismatch dislocations and defects near the interfaces between the layers, without a decrease in carrier mean-free paths, an increase in carrier scat-

 © 1978 The American Physical Society

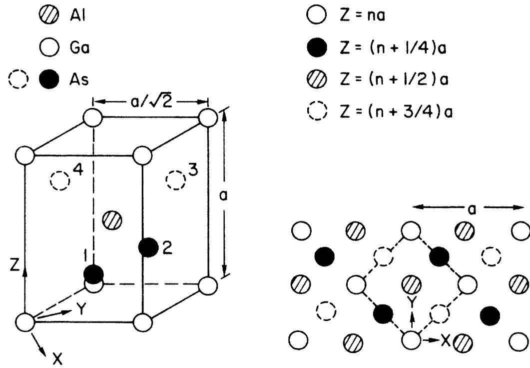

FIG. 1. Tetragonal unit cell of $(GaAs)_1$-$(AlAs)_1$. Coordinate axes are chosen along the edges of the GaAs fcc cell. The right half of the figure is a top view (along the [001] direction) with dashed lines showing boundaries of the unit cell.

tering, or an increase in nonradiative recombination rates. In the absence of this lattice constant matching the monolayer structure would not be formed at all.

The monolayer heterostructure is really a rather simple three-dimensional crystal. (It might be called $GaAlAs_2$.) It has space-group symmetry D_{2d}^1, a tetragonal unit cell with twice the volume of the GaAs unit cell, and four basis atoms with locations (0, 0, 0) for Ga, $(0, \frac{1}{2}a, \frac{1}{2}a)$ for Al, and $(\frac{1}{4}a, \frac{1}{4}a, \frac{1}{4}a)$ and $(\frac{1}{4}a, \frac{3}{4}a, \frac{3}{4}a)$ for As ($a = 5.64$ Å). Because there are twice as many atoms as in the ZB unit cell there will be twice as many valence electrons and twice as many energy bands.

The reciprocal-lattice basis vectors for this

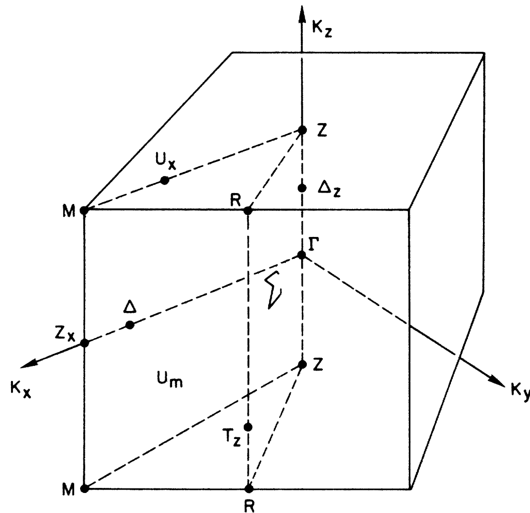

FIG. 2. Brillouin zone for $(GaAs)_1$-$(AlAs)_1$ showing the labeling of the high-symmetry points and lines. Shading indicates the reflection planes Σ and U_x.

TABLE I. Factor groups of points in the D_{2d}^1 Brillouin zone: symmetry operations.

E: (x,y,z); $2JC_4$: $(y,\bar{x},\bar{z})$, $(\bar{y},x,\bar{z})$
$2JC_2$: $(\bar{y},x,z)(y,x,z)$; $(JC_4)^2$: $(\bar{x},\bar{y},z)$
$2C_2$: $(x,\bar{y},\bar{z})(\bar{x},y,\bar{z})$

structure are $\vec{G}_1 = (2\pi/a)(1,1,0)$, $\vec{G}_2 = (2\pi/a) \times(-1,1,0)$, and $\vec{G}_3 = (2\pi/a)(0,0,1)$. A general reciprocal-lattice vector will have the form $\vec{G} = (2\pi/a)(n_1 - n_2, n_1 + n_2, n_3)$, where n_1, n_2, and n_3 may be any integers. Note that $n_1 - n_2$ and $n_1 + n_2$ will be both even or both odd.

The Brillouin zone (BZ) shown in Fig. 2 is one-half the size of the zinc-blende (ZB) BZ. It has two twofold rotation axes (k_x and k_y), one fourfold rotoinversion axis (k_z), and two mirror planes (R-M-Z_x-T_z-R and Γ-Z-R-T_z-Γ). The factor groups for the high-symmetry points and lines are given in Tables I and II. Note that if we replaced the Al atoms in Fig. 1 by Ga atoms, we would be performing calculations on the usual ZB structure, but with a unit cell twice the usual size, and a BZ one-half the usual size. In this case, the eigenvalues at any point in the reduced BZ could be found by folding the usual bands in half, e.g., the

TABLE II. Factor groups of points in the D_{2d}^1 Brillouin zone: factor groups.

Γ, Z, M, Z_x: D_{2d}						
D_{2d}	E	$(JC_4)^2$	$2JC_4$	$2C_2^1$	$2JC_2$	
Z_1, Γ_1	1	1	1	1	1	s
Z_2, Γ_2	1	1	1	−1	−1	
Z_3, Γ_3	1	1	−1	1	−1	
Z_4, Γ_4	1	1	−1	−1	1	z, xy
Z_5, Γ_5	2	−2	0	0	0	$(x,y), (xz,yz)$

Δ_z, T_z, U_z: S_4					
C_{2v}	E	$(JC_4)^2$	$(JC_2)_1$	$(JC_2)_2$	
T_1	1	1	1	1	s, z
T_2	1	1	−1	−1	
T_3	1	−1	1	−1	$x-y$
T_4	1	−1	−1	−1	$x+y$

Δ, U_x: C_{2x}			
C_{2x}	E	C_2	
Δ_1	1	1	s, x
Δ_2	1	−1	y, z

U_m, Σ: C_{1h}		
C_{1h}	E	JC_2
Σ_1	1	1
Σ_2	1	−1

eigenvalues at Γ in the reduced zone would be the eigenvalues from the ZB Γ and X points; Z_x and R would be equivalent to the ZB X and L points, respectively, with all degeneracies doubled. We will use these relations later on to discuss the effects of the unique $(GaAs)_1$-$(AlAs)_1$ structure.

For our calculations we have expressed the total crystal pseudopotential as a sum of atomic pseudopotential form factors

$$V(\vec{r}) = \sum_{\vec{G}} e^{i\vec{G}\cdot\vec{r}}[V_1(G) + V_2(G)e^{-i\vec{G}\cdot\vec{\tau}_0} + V_3(G) \times (e^{-i\vec{G}\cdot\vec{\tau}_1} + e^{-i\vec{G}\cdot\vec{\tau}_3})], \quad (1)$$

where $\vec{\tau}_0 = (0, \frac{1}{2}a, \frac{1}{2}a)$, $\vec{\tau}_1 = (\frac{1}{4}a, \frac{1}{4}a, \frac{1}{4}a)$, $\vec{\tau}_3 = (\frac{1}{4}a, \frac{3}{4}a, \frac{3}{4}a)$. For $(GaAs)_1$-$(AlAs)_1$, $V_1(G) = V_{Ga}(G)$, $V_2(G) = V_{Al}(G)$, and $V_3(G) = V_{As}(G)$, the atomic form factors given in Table III.

Our method of working with atomic form factors differs somewhat from the usual procedure of directly adjusting terms in the crystal pseudopotential of each pure material to fit optical data.[8-10] The present method has the advantage of being directly extendable to more complicated structures. In fact, it yields terms in the crystal pseudopotential which are quite similar to those of previous workers. Table IV contains a comparison. Note that while we have followed previous workers in requiring that $V(G)$ be zero for $G^2 \geq (2\pi/a)^2 16$, for $G^2 = (2\pi/a)^2 12$, we have not required that $V_{Ga}(G) = V_{Al}(G) = V_{As}(G)$ and $V_A(G) = 2[V_{cation}(G) - V_{anion}(G)] = 0$.

Our constraint that the arsenic form factors remain the same in both GaAs and AlAs calculations is an additional difference from previous work.

TABLE III. Pseudopotential form factors used throughout this calculation in Ry. The normalization volume is that of $(GaAs)_1$-$(AlAs)_1$, $\Omega = \frac{1}{2}a^3 = 605.95$ a.u.^{3}.

$(aG/2\pi)^2$	$V_{Ga}(G)$	$V_{Al}(G)$	$V_{As}(G)$
0	−0.1114	−0.1056	−0.1619
1	−0.0750	−0.0930	−0.1250
2	−0.0560	−0.0760	−0.0970
3	−0.0454	−0.0550	−0.0750
4	−0.0345	−0.0340	−0.0550
5	−0.0230	−0.0150	−0.0410
6	−0.0125	0.0025	−0.0270
7	−0.0030	0.0170	−0.0140
8	0.0063	0.0240	−0.0012
9	0.0160	0.0270	0.0060
10	0.0224	0.0260	0.0100
11	0.0241	0.0230	0.0125
12	0.0160	0.0200	0.0100
13	0.0060	0.0140	0.0090
14	0.0020	0.0080	0.0065
15	0.0	0.0020	0.0030
16	0.0	0.0	0.0

TABLE IV. Comparison of symmetric and antisymmetric zinc-blende pseudopotentials derived from the form factors of Table III to those used by previous workers. Superscripts are values of $(aG/2\pi)^2$. $V_S = 2(V_c + V_a)$, $V_A = 2(V_c - V_a)$, where c and a stand for cation and anion.

	GaAs			AlAs	
	This work	Ref. 8	Ref. 9	This work	Ref. 12
V_S^3	−0.2408	−0.245	−0.23	−0.2600	−0.2200
V_A^3	0.0592	0.062	0.07	0.0400	0.0725
V_A^4	0.0410	0.035	0.05	0.0420	0.0625
V_S^8	0.0102	−0.005	0.01	0.0456	0.0300
V_S^{11}	0.0731	0.075	0.06	0.0710	0.0700
V_A^{11}	0.0231	0.003	0.01	0.0210	−0.0075
V_A^{12}	0.012	0.0	0.0	0.0200	0.0

Previously, Hess *et al.*[10] found that an AlAs pseudopotential derived from pseudopotentials for AlSb, GaSb, and GaAs fit experiment rather poorly. Thus, the constraint that the same V_{As} be used in both calculations makes it necessary to find new potentials for both materials. This constraint also removes much of the arbitrariness which has been remarked on in connection with crystal pseudopotentials for ternary alloys.[11] In arriving at the set of form factors shown in Table III we examined scores of test potentials. Each set of $V_{Ga}(G)$, $V_{Al}(G)$, and $V_{As}(G)$ was tested for simultaneous agreement with the GaAs and AlAs band structures. We found no other set of form factors which fit the bands as well as these. Thus, we do not believe that there is another set of form factors which would give nearly the same fits to the pure materials and remarkably different results for monolayer heterostructures. As can be seen from Table V, eigenvalues calculated using our set of form factors agree rather well with previous calculations, including the self-consistent orthogonal-plane-wave (OPW) AlAs calculation of Stukel and Euwema.[12] Differences among these calculations are not expected to be as important as uncertainties due to neglect of spin-orbit coupling. Thus, in the recent nonlocal pseudopotential calculation of Chelikowsky and Cohen[13] the GaAs Γ_{15}^v level is split into a Γ_8^v at 0 eV and a Γ_7^v at −0.35 eV; the X_5^v is split into an X_7^v at −2.89 eV and an X_6^v at −2.29 eV; and the L_3^v is split into an $L_{4,5}^v$ at −1.20 eV and an L_6^v at −1.42 eV. In the latter two cases, degeneracies are not only split; pairs of levels are pushed downward substantially from their values in the local calculations shown in Table V. We believe these differences are primarily due to inclusion of spin-orbit rather than nonlocal effects.

TABLE V. Comparison of GaAs and AlAs high-symmetry eigenvalues to those of previous workers. Values from Ref. 8 and 9 have been read off energy-band diagrams and thus are approximate. All eigenvalues are in eV, measured from the valence-band maximum.

Symmetry	GaAs This work	GaAs Ref. 8	GaAs Ref. 9	AlAs This work	AlAs Ref. 10	AlAs Ref. 12
Γ_{15}^c	4.44	4.8	4.5	4.21	4.57	4.57
Γ_1^c	1.508	1.48	1.4	2.81	3.21	2.50
Γ_{15}^v	0.0	0.0	0.0	0.0	0.0	0.0
Γ_1^v	−12.05	−12.0		−11.57	−11.56	−11.48
X_3^c	2.37	2.55	2.1	2.89	2.62	2.86
X_1^c	1.972	2.2	1.8	2.21	2.25	2.38
X_5^v	−2.23	−2.0	−2.3	−2.32	−1.97	−2.01
X_3^v	−6.35	−6.2		−6.45	−5.55	−5.20
X_1^v	−9.83	−9.8		−8.96	−9.42	−9.61
L_3^c	5.15	5.5	5.0	4.93	5.15	5.25
L_1^c	1.802	1.8	1.7	2.48	2.76	2.57
L_3^v	−0.93	−0.9	−1.0	−0.98	−0.70	−0.80
L_2^v	−6.06	−6.0		−6.04	−5.52	−5.22
L_1^v	−10.52	−10.4		−9.85	−10.07	−10.14

Though these factors are important, our results appear sufficiently accurate for investigation of the structures we will be considering. In particular, our values for the lowest band gaps are in good agreement with experiment. At 2 °K the GaAs Γ_1^c-Γ_{15}^v gap is 1.519 eV,[14] the X_1^c-Γ_1^c separation is 0.462 eV, and L_1^c lies 0.17 ± 0.03 eV below X_1^c.[15] The AlAs X_1^c-Γ_{15}^v gap is 2.238 eV at ~0 °K;[16] Γ_1^c-Γ_{15}^v = 2.9 – 3.23 eV.[17-19] Our calculated results agree with experiment to better than 0.03 eV for the fundamental gaps and better than 0.1 eV for the next few higher gaps.

Because of our use of atomic form factors rather than direct crystal pseudopotential form factors to fit the energy bands of pure materials, it is straightforward to extend our treatment to alloys in Sec. IV through use of the virtual-crystal approximation.[7] The central idea of the VCA is that the correct one-electron potential of the actual configuration of atoms in the alloy can be replaced by an average potential over all possible configurations. For the crystalline alloy $Ga_{1-x}Al_xAs$ with ZB structure, a ZB potential is used with $V_{cation}(G) = (1-x)V_{Ga}(G) + xV_{Al}(G)$ and $V_{anion}(G) = V_{As}(G)$. For the $(Ga_{1-x}Al_xAs)_1$-$(Al_{1-x}Ga_xAs)$ monolayer heterostructure we use Eq. (1) with $V_1(G) = (1-x)V_{Ga}(G) + xV_{Al}(G)$, $V_2(G) = (1-x)V_{Al}(G) + xV_{Ga}(G)$, and $V_3(G) = V_{As}(G)$. For $(GaAs)_1$-$(Ga_{1-x}Al_xAs)_1$, we use $V_1(G) = V_{Ga}(G)$, $V_2(G) = (1-x)V_{Ga}(G) + xV_{Al}(G)$, and $V_3(G) = V_{As}(G)$. This process of weighting the potentials linearly with the probability of each atom's occupying a particular kind of site can be especially justified for $Ga_{1-x}Al_xAs$ alloys for the following reasons. The pseudopotential form factors depend not only on the composition but also on the volume normalization and dielectric screening of the alloy. (The VCA does not consider the variation of the dielectric screening.) Of all ZB semiconductors, only GaAs and AlAs have a close match in both lattice constants and dielectric constants [ϵ_0(GaAs) = 10.9,[20,21] 11.3,[22] ϵ_0(AlAs) = 10.3 (Ref. 22)]. It is reasonable to assume that both quantities remain unaltered while alloying in $Ga_{1-x}Al_xAs$. In addition, the short-range disorder in alloys is not expected to alter the shapes of density-of-states singularities predicted by the periodic potential of the VCA. Rather, a tailing of the spectrum into the forbidden gap is expected. According to an estimation based on electronegativities,[11] the effect of this aperiodicity should be less in $Ga_{1-x}Al_xAs$ than in any other ternary solid solution of the type $A_x^{III}B_y^{III}C_z^V$. Thus the use of the VCA in this paper does not encounter the serious drawbacks associated with its use in treating other ternary alloys.[11]

Given the pseudopotential form factors of Table III, the detailed calculation on the $(GaAs)_1$ – $(AlAs)_1$ structure follows methods developed for the treatment of simpler semiconductors. The pseudo wave functions of electrons at 60 points $\vec{k}$ in the BZ are expanded in a plane-wave basis set

$$\psi_{nk}(\vec{r}) = \sum_j a_j |\vec{K}_j\rangle, \quad (2)$$

where

$$|\vec{K}_j\rangle = |\vec{k} + \vec{G}_j\rangle. \quad (3)$$

At each $\vec{k}$, matrix elements of the pseudo Hamiltonian are found for ~200 values $|\vec{K}_j\rangle$ such that $|\vec{K}_j| \leq (27)^{1/2}(2\pi/a)$. Lowdin's perturbation scheme[23,24] is then used to reduce the size of the secular equation to $N \leq 100$, where N is chosen such that $|\vec{K}_{j>N}| > |\vec{K}_{j\leq N}|$. Eigenvalues and eigenvectors of the perturbed matrix (which is complex for general points in the BZ) are found by standard numerical techniques. The numerical uncertainty in the eigenvalues, coming primarily from the perturbation theory, is estimated to be ≤0.02 eV. Differences between energy levels should be accurate to ~0.05 eV.

In order to find the imaginary part of the dielectric function $\epsilon_2(\omega)$ the density of states $N(E)$, and the charge density $\rho(\vec{r})$, we calculate the oscillator strengths $\langle\psi_{ik}|\hat{P}_z|\psi_{jk}\rangle$, $\langle\psi_{ik}|(\hat{p}_x+\hat{p}_y)/\sqrt{2}|\psi_{jk}\rangle$ for all valence to conduction transitions and the contributions $\psi^*_{ik}\psi_{ik}$ to $\rho(\vec{G})$ from all occupied eigenstates ψ_{ik}, k ranging over 60 points on a fine mesh in $\frac{1}{8}$ of the BZ. Integrations for

$$\epsilon_2(\omega)\omega^2 = \left(\frac{2\pi e}{m}\right)^2 \hbar \sum_{ij} \int_{BZ} \frac{2}{(2\pi)^3} |\langle\psi_{i\vec{k}}|\hat{p}|\psi_{j\vec{k}}\rangle|^2 \times \delta(\omega - E_{j\vec{k}} + E_{i\vec{k}}) d\vec{k} \quad (4)$$

and

$$N(E) = \sum_{i=1}^{8} \int_{BZ} \delta(E - E_{i\vec{k}}) d\vec{k}, \quad (5)$$

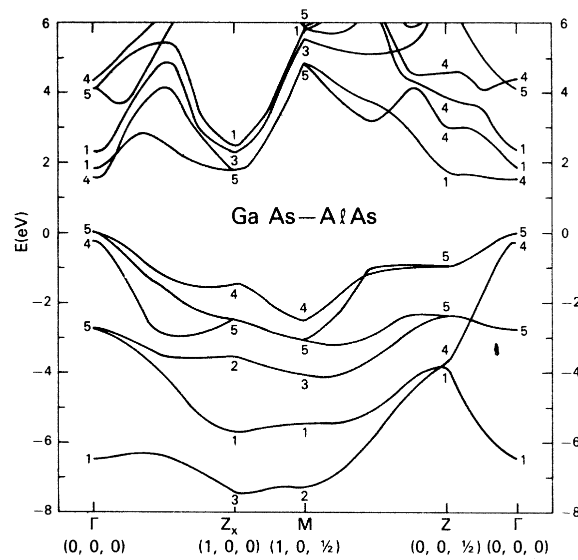

FIG. 3. Energy bands of $(GaAs)_1$-$(AlAs)_1$ along the most important high-symmetry lines. (Lowest two valence bands are omitted).

were performed by the Monte Carlo method of summing quantities evaluated by cubic interpolation[24] at 12 000 random points in the $\frac{1}{8}$ of the BZ given in Fig. 2.

III. ELECTRONIC PROPERTIES OF $(GaAs)_1$-$(AlAs)_1$

A. Energy-band structure

Energy bands for the $(GaAs)_1$-$(AlAs)_1$ monolayer heterostructure are shown in Figs. 3 and 4 for all

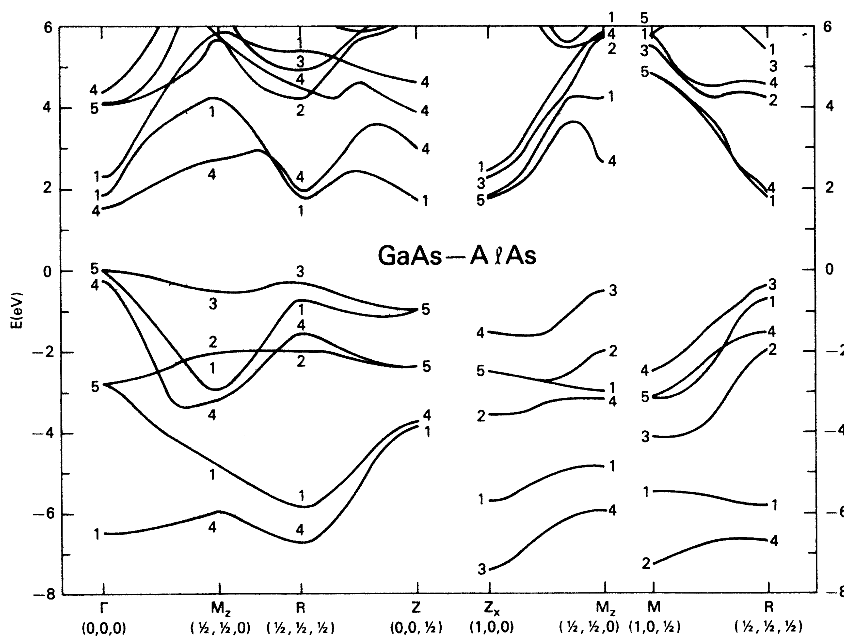

FIG. 4. Energy bands of $(GaAs)_1$-$(AlAs)_1$ along all high-symmetry lines not shown in Fig. 3. (Lowest two valence bands are omitted.)

TABLE VI. Prominent critical points and their oscillator strengths for the electronic spectrum.

I–J	$(a/2\pi)\vec{K}$	$E_J - E_I$ (eV)	$\lvert P_z\rvert^2$	$\lvert p_\perp\rvert^2$	Symmetry
8–9	(0, 0, 0)	1.58	0	0	M_0
	$(0, 0, \frac{1}{2})$	2.67	0	0.019	M_1
	(1, 0, 0)	3.36	0	0.094	M_0
	$(\frac{1}{2}, \frac{1}{4}, \frac{1}{2})$	3.59	0.0167	0.005	M_0
	$(\frac{3}{8}, \frac{1}{8}, \frac{1}{4})$	3.73	0.096	0.050	M_2
	$(\frac{1}{2}, 0, 0)$	3.78	0.186	0.012	M_1
	$(\frac{5}{8}, \frac{1}{8}, 0)$	3.88	0.119	0.022	M_1
	$(\frac{3}{8}, \frac{1}{8}, \frac{1}{2})$	3.97	0.033	0.022	M_3
	$\sim(\frac{3}{4}, \frac{1}{4}, \frac{1}{4})$	~4.04	0.224	0.004	M_2
	$\sim(\frac{3}{4}, 0, \frac{1}{4})$	~4.3	0.166	0.081	M_2
	$(\frac{5}{8}, \frac{1}{8}, \frac{1}{4})$	4.37	0.126	0.036	M_2
	$(\frac{5}{8}, \frac{1}{8}, \frac{1}{2})$	4.50	0.205	0.002	M_3
	$\sim(\frac{1}{2}, 0, \frac{1}{4})$	~4.75	0.022	0.060	M_3
8–10	(0, 0, 0)	1.88	0	0.036	M_0
	$\sim(\frac{1}{8}, \frac{1}{8}, \frac{1}{4})$	3.58	0.136	0.093	M_1
	$\sim(\frac{1}{4}, \frac{1}{4}, \frac{1}{4})$	~3.72	0.193	0.104	M_1
	$(\frac{1}{2}, \frac{1}{4}, \frac{1}{2})$	3.86	0.041	0.059	M_0
	$(\frac{5}{8}, \frac{3}{8}, \frac{1}{4})$	4.08	0.123	0	M_1
	$(\frac{3}{8}, \frac{1}{8}, 0)$	4.09	0.106	0.004	M_0
	$(\frac{3}{8}, \frac{1}{8}, \frac{1}{4})$	4.26	0.069	0.044	M_1
	$(\frac{5}{8}, \frac{1}{8}, \frac{1}{4})$	4.47	0.065	0.057	M_1
	$(\frac{1}{2}, \frac{1}{4}, 0)$	4.62	0.058	0.007	M_1
	$(\frac{1}{4}, 0, \frac{1}{2})$	4.99	0	0.045	M_3
	$(\frac{5}{8}, \frac{1}{8}, 0)$	5.13	0.06	0.08	M_3
	$(\frac{1}{2}, 0, 0)$	5.43	0.04	0.08	M_3
8–11	(0, 0, 0)	2.39	0	0.017	M_0
	(1, 0, 0)	3.82	0.280	0	M_0
	$(0, 0, \frac{1}{2})$	4.89	0	0.120	M_1
	$(\frac{5}{8}, \frac{3}{8}, \frac{1}{4})$	4.93	0	0.045	M_0
	$\sim(\frac{3}{8}, \frac{1}{8}, \frac{1}{2})$	5.23	0.149	0.009	M_1
	$(\frac{1}{2}, \frac{1}{4}, \frac{1}{2})$	5.29	0.013	0.04	M_2
	$(\frac{1}{2}, 0, \frac{1}{4})$	5.81	0.181	0.022	M_2
6–11	(0, 0, 0)	2.57	0.079	0	M_0
	$(\frac{1}{2}, \frac{1}{2}, \frac{1}{2})$	5.73	0.288	0	M_0
	$(\frac{5}{8}, \frac{3}{8}, \frac{1}{4})$	6.20	0.111	0	M_0
	$(0, 0, \frac{1}{2})$	6.21	0	0.05	M_1
	$(\frac{1}{2}, \frac{1}{4}, \frac{1}{2})$	6.46	0.061	0.003	M_0
	$(\frac{1}{4}, \frac{1}{4}, \frac{1}{2})$	6.75	0.171	0.001	M_1
	$(\frac{3}{8}, \frac{1}{8}, \frac{1}{4})$	6.99	0.034	0.006	M_2
	$(\frac{1}{4}, \frac{1}{4}, \frac{1}{4})$	7.21	0.036	0.010	M_3
	$\sim(\frac{1}{2}, 0, \frac{1}{4})$	7.32	0.027	0.014	M_2
	$(\frac{1}{2}, 0, 0)$	7.88	0.027	0.020	M_3
6–12	$(\frac{5}{8}, \frac{3}{8}, \frac{1}{2})$	6.31	0.191	0	M_0
7–10	(0, 0, 0)	1.88	0	0.189	M_0
	$(\frac{1}{2}, \frac{1}{2}, \frac{1}{2})$	2.61	0.299	0	M_0
	$(\frac{1}{4}, \frac{1}{4}, \frac{1}{4})$	3.51	0.137	0.073	M_0
	(1, 0, 0)	4.33	0.035	0	M_0
	$\sim(\frac{1}{2}, 0, \frac{1}{2})$	~4.87	0.258	0.001	M_1
	$(\frac{5}{8}, \frac{1}{8}, \frac{1}{4})$	4.98	0.084	0.018	M_0
	$(\frac{3}{4}, \frac{1}{4}, \frac{1}{4})$	5.02	0.217	0.003	M_1
	$\sim(\frac{5}{8}, \frac{3}{8}, \frac{1}{4})$	~5.31	0.051	0	M_2
	$\sim(\frac{5}{8}, \frac{1}{8}, \frac{1}{2})$	~5.31	0.204	0.009	M_3
	$(\frac{1}{2}, 0, 0)$	5.77	0.175	0.025	M_2
	$(\frac{5}{8}, \frac{3}{8}, 0)$	6.68	0.101	0	M_3
7–12	$(\frac{1}{4}, 0, \frac{1}{2})$	5.54	0	0.109	M_1
	$(\frac{1}{8}, \frac{1}{8}, \frac{1}{2})$	5.94	0.014	0.247	M_2
8–12	$(0, 0, \frac{1}{4})$	4.52	0	0.238	M_1
	$(0, 0, \frac{1}{2})$	5.71	0	0.218	M_2
	$\sim(\frac{1}{8}, \frac{1}{8}, \frac{1}{4})$	4.96	0.041	0.190	M_3
6–10	(0, 0, 0)	2.06	0.253	0	M_0
	$(0, 0, \frac{1}{2})$	5.38	0	0.111	M_2

high-symmetry lines in the D_{2d}^1 BZ. The lowest pair of bands have energies between -12.01 and -9.5 eV and have been omitted from these figures. We have used the GaAs valence-band maximum as our zero of energy. The $(GaAs)_1$-$(AlAs)_1$ valence-band maximum is at Γ and is $+0.034$ eV. Because this unit cell is twice the ZB unit cell, there are twice as many bands as in the usual ZB semiconductor. This results in more band crossings and repulsions and produces more complicated bands. The [100] and [010] directions in this structure are not equivalent to the [001] direction. The conduction-band minimum at $(0,0,1)(\pi/a)$ is 0.85 eV below the conduction-band minimum at $(1,0,0)(\pi/a)$.

The lowest conduction-band minima lie along the [0 0 1] direction (parallel to the heterostructure

axis). The Γ_4 minimum is at 1.619 eV, giving a minimum direct gap at 1.585 eV. The Z_1 minimum is at 1.743 and the absolute minimum is 1.587 eV at $(0\ 0\ \frac{1}{8})(2\pi/a)$. Since this last value differs from the Γ_4 minimum by only 0.03 eV (less than the numerical uncertainty in the calculation) we believe that this is probably a direct-gap material. This gap is 0.32–0.42 eV less than the (indirect) gap in the alloy of the same composition.[25] (For further comparisons to the alloy, see Sec. IV.)

Other important conduction-band minima are at R (1.869 and 1.959 eV), Γ_1 (1.914 eV), and Z_{X5} (1.931 eV). The R minima arise from the Z.B. L_1^c level; the Γ_1 minimum comes from the ZB Γ_1^c level; both the Γ_4 and Z_{X5} conduction-band minima arise from the ZB X_1^c level. In $Ga_{0.5}Al_{0.5}As$ the X_1^c level lies at about 1.95 eV. The heterostructure ordering of the Ga and Al cations onto alternating monolayers produces a splitting of the Γ_4^c and Z_{X5}^c levels as well as a lowering of both relative to the alloy X_1^c level. The size of this effect cannot be determined from symmetry or other *a priori* considerations. An accurate pseudopotential is therefore essential for determining the ordering and the absolute energies of the various conduction-band minima. As discussed above, our form factors fit the energy bands of GaAs and AlAs very accurately. As will be seen in Sec. IV, these same form factors also fit the $Ga_{1-x}Al_xAs$ alloy over the entire range $0 \leq x \leq 1$. We are therefore confident that Γ_4^c lies below Z_{X5}^c, Z_1^c and all the higher conduction-band minima, making $(GaAs)_1$-$(AlAs)_1$ a direct (or very nearly direct) material.

The calculated oscillator strengths (OS) reveal an important point about the Γ_5^v-Γ_4^c band gap. Because the Γ_5 and Γ_4 levels are, by symmetry, primarily of p character, optical transitions across this gap will be very weak. Only the presence of a slight amount of d character in the Γ_4^c level keeps the transition from being completely forbidden. The Γ_5^v-Γ_4^c and Γ_5^v-Γ_1^c oscillator strengths are compared in Table VI. The OS for Γ_5^v-Γ_4^c is negligible. This will make the Γ_4^c minimum very difficult to detect experimentally. In this respect $(GaAs)_1$-$(AlAs)_1$ is very different from III-V and II-VI zinc-blende, wurtzite, and rocksalt semiconductors. Recent calculations on α-quartz[26] and β-cristobalite[27] showed dipole forbidden lowest interband transitions, but SiO_2 has a much wider band gap (~9–10 eV) and the forbidden transitions involve oxygen lone-pair valence states. Thus, the present result for $(GaAs)_1$-$(AlAs)_1$ is unexpected.

B. Optical spectrum ϵ_2

As the optical spectra in Fig. 5 show, the lowest peak which is likely to be observable by techniques like optical absorption is at about 1.89 eV. The inset of Fig. 5 shows details of $\epsilon_2\omega^2$ near the absorption edge. The edge at 1.88 eV for light polarized normal to the heterostructure axis comes from Γ_5^v-Γ_1^c transitions. We have calculated an optical-absorption coefficient of $\sim 0.23 \times 10^{+4}$ cm^{-1} for the 1.89-eV peak, as compared to a value of $\sim 8.5 \times 10^4$ cm^{-1} for the peak at 4.1 eV. The 2.06-eV edge for parallel polarized light comes from Γ_4^v-Γ_1^c transitions.

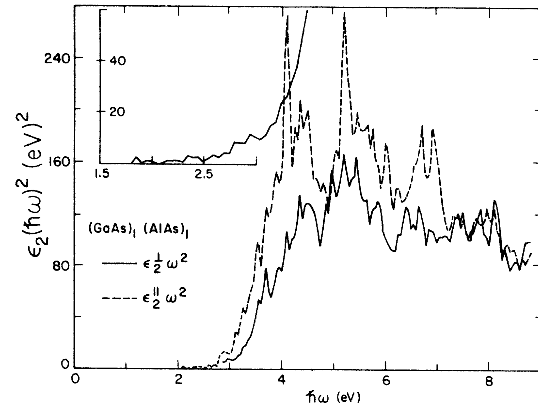

FIG. 5. Optical spectra $\epsilon_2^{\perp}\omega^2$ (solid line) and $\epsilon_2^{\parallel}\omega^2$ (broken line) of $(GaAs)_1$-$(AlAs)_1$. The inset shows more detail of $\epsilon_2^{\perp}\omega^2$ near the absorption edge.

A comparison of the $I^{\parallel}(\omega) \equiv \epsilon_2^{\parallel}\omega^2$ and $I^{\perp}(\omega) \equiv \epsilon_2^{\perp}\omega^2$ spectra shows strong polarization effects accompanied by alternation of intensities. For the $\epsilon_2^{\parallel}\omega^2$ spectrum $I^{\parallel}(4.10) > I^{\parallel}(4.5)$, $I^{\parallel}(5.25) > I^{\parallel}(5.5)$, and $I^{\parallel}(6.7) = I^{\parallel}(6.9)$. For the $\epsilon_2^{\perp}\omega^2$ spectrum, $I^{\perp}(4.1) < I^{\perp}(4.5)$, $I^{\perp}(6.7) > I^{\perp}(6.9)$, and $I^{\perp}(5.25) = I^{\perp}(5.5)$.

Because $(GaAs)_1$-$(AlAs)_1$ contains twice as many bands as GaAs, its optical spectra contain at least four times as many critical points (CP). To facilitate CP discussion we have decomposed the complete $\epsilon_2^{\parallel}\omega^2$ spectrum into a superposition of spectra from pairs of bands. The most important of these pair spectra are shown in Fig. 6. From these we conclude that the structures in the region $E_c - E_v < 4.5$ eV are associated with $8 \to 9$, $8 \to 10$, and $7 \to 10$ transitions; those in the region $4.5 < E_c - E_v < 6$ eV with $7 \to 10$, $7 \to 11$, and $8 \to 11$ transitions; and those in the region $6 < E_c - E_v < 8$ eV with $6 \to 11$, $6 \to 12$, $7 \to 12$, $7 \to 13$, and $7 \to 14$ transitions.

Because even the pair spectra of Fig. 6 are extremely complicated, we made a complete CP analysis for each edge, peak, and shoulder. Table VI contains part of this CP analysis, but because of space limitations the greater part of the analysis has been omitted. The most important results of this analysis may be summarized as follows. (i) Polarization effects are large as the oscillator strengths (OS) $|p_z|^2$ and $|p_\perp|^2$ are quite different at a given critical point. (ii) Contrary to the case

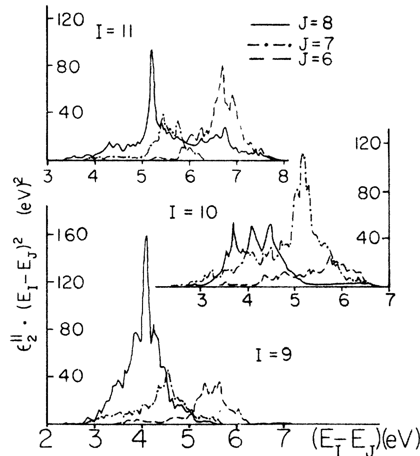

FIG. 6. Most important interband transitions which contribute to $\epsilon_2^{\parallel}\omega^2$. In each case, J is the index of the valence level (8 being the uppermost) and I is the index of the conduction band (9 being the lowest).

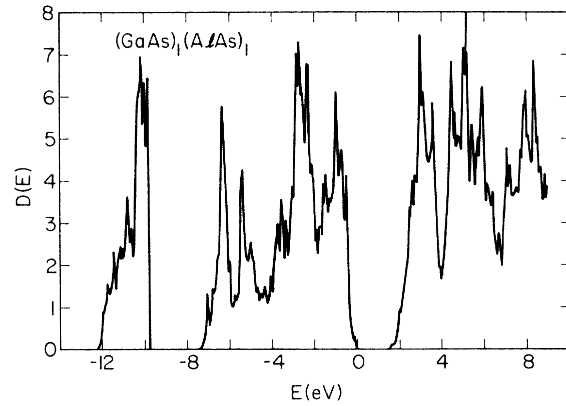

FIG. 7. Density of states for $(GaAs)_1$-$(AlAs)_1$. States below $E = 0.03$ belong to the valence band, while states above belong to the conduction band.

in cubic NaCl or ZB semiconductors, the average value of the OS for a given pair of bands is frequently larger than at high-symmetry points or along symmetry lines. Thus, contributions to ϵ_2 structures come mainly from general points in the BZ. (iii) The OS $|p_z|^2$ for transitions below 2 eV are extremely small. The OS $|p_\perp|^2$ becomes significant only at 1.87 eV, the onset of optical absorption. The 1.59-eV transition across the smallest direct gap is therefore unobservable, as mentioned above.

Figure 5 is somewhat similar to the ϵ_2 of pure GaAs given in Ref. 8. The group of structures for $\hbar\omega < 4.5$ eV corresponds to the first peak between 3 and 4 eV in GaAs which comes mainly from the $4 \rightarrow 5$ transition. The structures between 4.5 and 6.0 eV in Fig. 5 correspond to the second peak, between 4 and 6 eV in GaAs, which comes from $4 \rightarrow 5$ and $4 \rightarrow 6$ transitions. The structures between 6 and 8 eV in Fig. 5 correspond to the peak at 6–7 eV in GaAs, which comes from $4 \rightarrow 6$, $3 \rightarrow 6$, and $4 \rightarrow 7$ transitions. Note that the (5,6), (7,8), (9,10), (11,12), and (13,14) bands in $(GaAs)_1$-$(AlAs)_1$ come from the 3, 4, 5, 6, and 7 Z.B. bands, respectively. The III–V ZB materials are known to have similar ϵ_2 spectra.[8,12] It is not surprising that $(GaAs)_1$-$(AlAs)_1$ has similar gross features. However, there are extra fine structures coming from the doubled number of bands in the monolayer heterostructures. These extra structures should be observable by electroreflectance measurements in the range 4.0 eV $\leq \hbar\omega \leq$ 8.0 eV.

C. Electron density of states

The calculated density of states (DOS) for $(GaAs)_1$-$(AlAs)_1$ is shown in Fig. 7. It contains three separated portions, the lower two arising from the valence band, and the topmost from the conduction band. In their widths the lower two portions look like superpositions of densities of states for pure GaAs and AlAs. The lowest portion (−12.05 to −9.58 eV) comes from the two lowest valence bands. Its width is 2.46 eV, compared to widths of 2.23 eV for GaAs and 2.6 eV for AlAs. The charge associated with this portion of the DOS is greatest on As sites and extends in bonding lobes toward the cation positions. (Charge at the cation sites is small, but not zero.) The second portion of the DOS (−7.4 to 0.03 eV) is strongly bonding in character; it comes from the six highest valence bands. It is wider (7.43 eV) than analogous portions of the GaAs and AlAs curves (6.35 and 6.45 eV, respectively). Half of this broadening can be attributed to the difference in valence-band edges in the pure materials (0.0 for GaAs, −0.32 eV for AlAs); the rest must be attributed to the altered crystal structure in $(GaAs)_1$-$(AlAs)_1$. The gap between these portions of the DOS is 2.2 eV compared to 3.48 eV for GaAs and 2.51 eV for AlAs. The total valence-band width is 12.1 eV compared to 12.05 eV for GaAs and 11.57 eV for AlAs.

In the first column of Table VII are listed the energies and symmetries of the prominent valence-band DOS features. There are about twice as many peaks and valleys in this DOS as there are for GaAs. The next two columns of Table VII list energies and symmetries of GaAs and AlAs which are "parents" to the $(GaAs)_1$-$(AlAs)_1$ DOS structures. That is, these are the energies of GaAs and AlAs high-symmetry points which, if the ZB BZ is folded in half, give rise to the monolayer symmetries of column 1. Which ZB L-point symmetries correspond to which R-point monolayer symmetries, for example, can be deduced from a comparison of character tables. Analysis of compar-

TABLE VII. Energies and symmetries for prominent structures of the valence-band density of states of $(GaAs)_1$-$(AlAs)_1$ related to parent structures in pure GaAs and AlAs and compared to structures for $Ga_{0.5}Al_{0.5}As$ and $(Ga_{0.7}Al_{0.3}As)_1$-$(Al_{0.7}Ga_{0.3}As)_1$. Representations in parentheses following $(GaAs)_1$-$(AlAs)_1$ and $(Ga_{0.7}Al_{0.3}As)_{0.1}$-$(Al_{0.7}Ga_{0.3}As)_1$ energies are appropriate to the monolayer structures. Representations for GaAs, AlAs, and $Ga_{0.5}Al_{0.5}As$ are for zincblende structure.

$(GaAs)_1$-$(AlAs)_1$	GaAs	AlAs	$Ga_{0.5}Al_{0.5}As$	$(Ga_{0.7}Al_{0.3}As)_1$-$(Al_{0.7}Ga_{0.3}As)_1$
-12.05 (Γ_1)	-12.05 (Γ_1)	-11.89 (Γ_1)	-11.94 (Γ_1)	-11.96 (Γ_1)
-10.62 (R_4)	-10.52 (L_2)		-10.31 (L_2)	-10.41 (R_4)
-10.18 (R_1)		-10.17 (L_2)		-10.25 (R_1)
-9.60 (Γ_4)	-9.83 (X_1)		-9.53 (X_1)	-9.54 (Γ_4)
-9.58 (Z_{X5})		-9.28 (X_1)		-9.54 (Z_{X5})
-6.64 (R_4)		-6.35 (L_1)	-6.20 (L_1)	-6.37 (R_4)
-5.88 (R_1)	-6.06 (L_1)			-6.16 (R_1)
-6.51 (Γ_1)		-6.77 (X_3)	-6.55 (X_3)	-6.55 (Γ_1)
-5.80 (Z_{X1})	-6.35 (X_3)			-6.24 (Z_{X1})
-3.47 (Z_{X2})		-2.63 (X_5)	-2.42 (X_5)	-2.83 (Z_{X2})
-2.64 (Γ_5)	-2.23 (X_5)			-2.44 (Γ_5)
-0.65 (R_1)		-1.30 (L_3)	-1.10 (L_3)	-0.91 (R_1)
-0.37 (R_3)	-0.93 (L_3)			-0.78 (R_3)
-0.14 (Γ_4)		-0.32 (Γ_{15})	-0.14 (Γ_{15})	-0.13 (Γ_4)
0.03 (Γ_5)	0.0 (Γ_{15})			-0.09 (Γ_5)

ative wave functions will be given shortly. However, we would first like to make this point that the $(GaAs)_1$-$(AlAs)_1$ DOS is very nearly a superposition of structures from GaAs and AlAs. However, there are important effects which arise from the unique arrangement of atoms in $(GaAs)_1$-$(AlAs)_1$. These effects are most significant for higher levels in the valence band. Some pieces of structure near the valence-band edge are moved by more than 0.5 eV. Also, individual levels are not pure GaAs bonds or pure AlAs bonds. Analysis of wave functions $\psi_{n\vec{k}}(\vec{r})$ for valence levels at Γ, Z_x, and R shows that most levels contribute charge to regions surrounding Ga, Al, and As. Detailed consideration of these wave functions shows how the structures in the $(GaAs)_1$-$(AlAs)_1$ DOS arise from the GaAs and AlAs structures shown in Table VII.

The R_1 level is p-like about Al and As_3 and s-like about Ga and As_1, while the R_4 level has the opposite atomic character. The lowest L_2 levels in pure GaAs and AlAs are predominently p-like about the cations and s-like about the As, while the lowest L_1 levels are predominently s-like about the cations and s-p hybridized about As.[28] Thus, the -10.62-eV R_4 and -10.18-eV R_1 levels come from the lowest L_2 levels of pure GaAs and AlAs, respectively; the -6.64-eV R_4 level and the -5.88-eV R_1 level come from AlAs and GaAs L_1 levels, respectively. The upper L_3 levels in GaAs and AlAs are p-like about the cations and the R_3 level at -0.37 eV is s-like about Al and p-like about Ga. Thus, though their energies are shifted by 0.56 and 0.65 eV, the -0.37-eV R_3 and -0.65-eV R_1 clearly come from the GaAs and AlAs L_3 levels shown. Similar analyses confirm the origins assigned to the Γ and Z_x levels in Table VII. The last two columns of Table VII contain results for related alloys. These results will be discussed in Sec. IV, as will implications for experimental comparison of these materials.

Density-of-states structures coming from levels predominantly Al-like in character have a substantially greater DOS than those which are predominantly Ga-like. This rule is reversed for levels derived from the ZB X point. For example, $\Gamma_4(X_1) = -9.60$ eV and $Z_{X1}(X_3) = -5.80$ eV are Ga-like and contribute more to the DOS than the $Z_{X5}(X_1) = -9.58$ eV and $\Gamma_1(X_3) = -6.51$ eV, which are Al-like.

D. Electron charge density

The sum of all contributions to $\rho(\vec{r})$ is shown in Fig. 8 for a plane which includes both Ga-As and Al-As bonds. Bonding-charge maxima (BCM) are located along lines joining cation to anion, and are somewhat closer to the anions, in agreement with previous III-V and II-VI charge-density calculations.[13,29] The AlAs BCM is greater than that of GaAs in agreement with the greater covalency of AlAs derived from the dielectric theory of Phillips and Van Vechten.[22,30] A higher BCM for AlAs can also be predicted from the polarity theory of Harrison and Ciraci.[31] Since the Ga-As BCM shown here is almost exactly that found in the nonlocal GaAs calculation,[13] there is apparently no charge transfer from one kind of bond to the other.

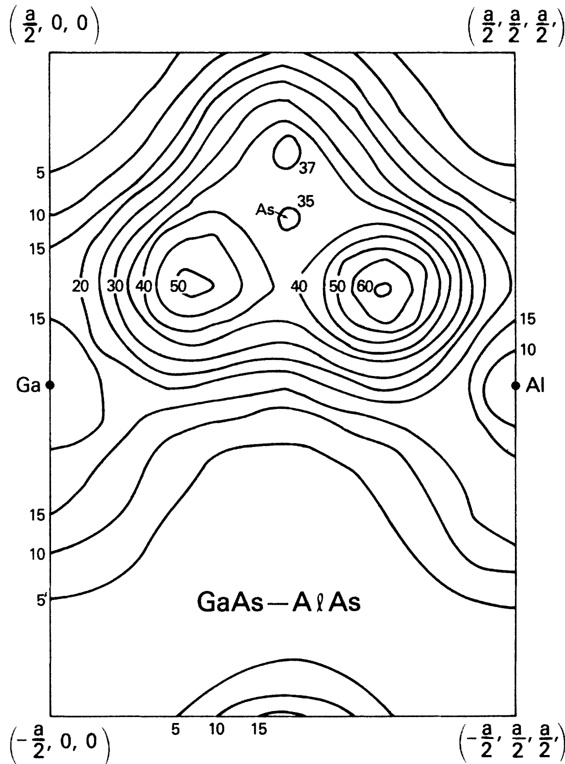

FIG. 8. Valence-charge density $\rho(\vec{r})$ of $(GaAs)_1$-$(AlAs)_1$. All values of the charge are in electrons per $(GaAs)_1$-$(AlAs)_1$ unit cell (twice the size of the zinc-blende unit cell).

If we divide the unit cell into region I which is nearest the Ga site, region II nearest the Al site, and region III nearest to one or the other As sites, we find that the total charge of 16 electrons is divided into $Z_{\rm I}=3.12$, $Z_{\rm II}=3.67$, and $Z_{\rm III}=9.21$ [$=2(4.605)$]. That there should be more charge on Al than on Ga is also in agreement with the less ionic, more covalent nature of the Al-As bond.

IV. VIRTUAL-CRYSTAL APPROXIMATION CALCULATIONS ON ALLOYS

As mentioned in Sec. I, the $(GaAs)_1$-$(AlAs)_1$ materials which have been produced recently are characterized by ~30% "islandlike" disorder.[3,5] Therefore, the connection between our calculations on ideal structures and measurements on as-grown structures is somewhat unclear. In order to make somewhat closer comparison with experiment, we need to include the effects of compositional disorder in our calculation. Such effects are included through adoption of the VCA as discussed in Sec. II. We use the VCA to treat three types of materials.

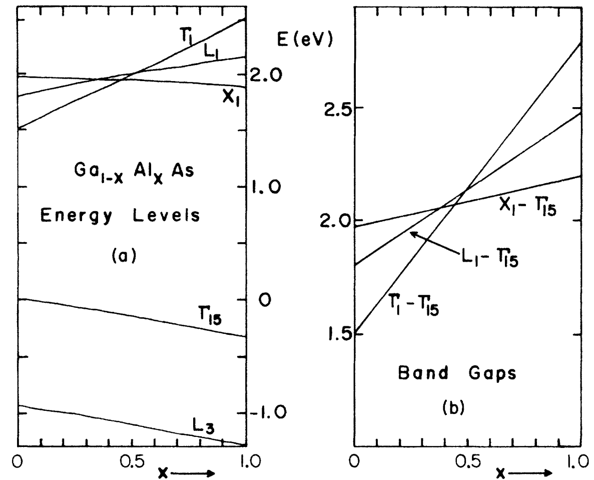

FIG. 9. (a) Composition dependence of the most important valence and conduction levels of the zinc-blende alloy $Ga_{1-x}Al_xAs$; (b) compositon dependence of the most important $Ga_{1-x}Al_xAs$ band gaps.

A. $Ga_{1-x}Al_xAs$ zinc-blende alloy

In order to show how the VCA is used, and to explore its usefulness for treating the alloy monolayer heterostructures of Secs. IV B and IV C, we have first performed a calculation on the ternary $Ga_{1-x}Al_xAs$ alloy. This is a substitutional alloy with perfect ZB structure, but with cation sites having a probability $1-x$ of being occupied by a Ga atom and a probability x of being occupied by an Al atom. The form factors for this alloy are given in Sec. II. In Fig. 9(a) we show the composition dependence of two valence-band maxima and three conduction-band minima for this alloy. (The zero of energy in this figure was taken at the GaAs valence-band maximum.) As can be seen, all levels depend nearly linearly on composition. Departures from linearity have the form of an upward bowing of all levels. That is, $E_i^x=E_i^{0.0}+bx+cx^2$, $b \gtrsim E_i^{1.0}-E_i^{0.0}$, $c<0.0$. There is a very slight downward bowing to the composition dependence of the principal band gaps (~1–5 meV), in agreement with general trends in ternary alloys[11] and with experimental measurements on $Ga_{1-x}Al_xAs$,[32,33] but this is not visible in Fig. 9(b). In this respect our use of the VCA is substantially more successful than early VCA work on $GaAs_{1-x}P_x$ and other ternary alloys which consistently showed upward bowing of band gaps.[11] This is probably due primarily to the great similarity of GaAs and AlAs lattice constants and dielectric constants. Our value of x for the crossover from direct to indirect gap alloys is $x_c=0.45$ in good agreement with the recent experimental value of $x_c=0.43$.[34] Our value of the energy gap at crossover $E_{gc}=2.07$ eV is again in good

agreement with the experimentally deduced values $E_{gc} = 2.06$.[33] Our values for the valence-band discontinuity between GaAs and $Ga_{1-x}Al_xAs$ are -0.055, -0.144, -0.244, and -0.315 eV for $x = 0.2$, 0.5, 0.8, and 1.0, respectively. The value of -0.26 eV for $x = 1$ predicted by Frensley and Kroemer[35] is in reasonable agreement with our result.

For $x = 0.5$, there is some spread in experimental values of the lowest-energy gap: ~2,[25] 1.9–2.0,[11] ~1.98,[3] and 2.07.[33] Our value is 2.09 eV. These differences may be due to the different temperatures at which measurements were made, or it may be that differently prepared samples have different degrees of randomness. This particular composition is important because differences in properties of $(GaAs)_1$-$(AlAs)_1$ and $Ga_{0.5}Al_{0.5}As$ are a way of proving that the desired monolayer ordering is present.[3,5] As noted in Sec. III, our minimum $(GaAs)_1$-$(AlAs)_1$ band gap is 1.59 eV, considerably less than any plausible value of the $Ga_{0.5}Al_{0.5}As$ band gap. This large difference results from the ordering of the Ga and Al atoms into alternating layers. This ordering changes the potential in such a way that the Γ_4^c and Γ_1^c levels are moved farther apart than they would be in the $x = 0.5$ alloy, and both levels are lower than they otherwise would be. There is a similar separation of the highest two Γ_5^v levels. Thus, the conduction-band minimum is about 0.3 eV lower, and the band gap is about 0.5 eV narrower than in the $Ga_{0.5}Al_{0.5}As$ alloy. Additionally, the $(GaAs)_1$-$(AlAs)_1$ band gap is direct, whereas the lowest $Ga_{0.5}Al_{0.5}As$ gap is indirect. All these are distinguishing characteristics of the monolayer material. However, because of the matrix element effects discussed in Sec. III, it is very difficult to distinguish $(GaAs)_1$-$(AlAs)_1$ from $Ga_{0.5}$-$Al_{0.5}As$ by optical techniques. Measurements of the 30% disordered monolayer material indicated a band gap of ~2.06 eV, actually ~0.07-eV *greater* than the alloy gaps which were measured simultaneously.[3,4] Our calculated optical-absorption edge for the $(GaAs)_1$-$(AlAs)_1$ is ~0.2 eV less than the measured value for the band gap. We believe that this discrepancy arises from the disorder in the MBE prepared monolayer materials. The dependence of the band gap on disorder will be taken up again in Sec. V B, in connection with our discussion of disorder.

Although optical-absorption-edge measurements cannot easily distinguish $(GaAs)_1$-$(AlAs)_1$ from $Ga_{0.5}Al_{0.5}As$, optical measurements at higher energies will certainly reveal distinctions. As discussed above, there are strong polarization effects and, between 4 and 8 eV, the monolayer $\epsilon_2^{\parallel}$ and $\epsilon_2^{\perp}$ both contain twice the structure of the ZB ϵ_2. The alloy ϵ_2 will show no polarization effects. It is expected to have essentially the same structure as the ZB, with peak positions which are averages of the GaAs and AlAs peak positions. Optical measurements of peak splittings and polarization effects above 4 eV will then provide a measure of monolayer ordering.

A more sensitive method of distinguishing $(GaAs)_1$-$(AlAs)_1$ from $Ga_{0.5}Al_{0.5}As$ may be provided by photoemission measurements of the valence-band DOS. The monolayer ordering doubles the number of peaks in the ZB DOS. Values for the $Ga_{0.5}Al_{0.5}As$ structures are given in the fourth column of Table VII. For $E < -5.0$ eV, the separation of the peaks which originated from the same peak in Z.B. may be as much as 0.8 eV. For $0.0 \geq E \geq -5.0$ eV, structures are not only split by 0.2–0.8 eV, they are moved by as much as 0.6 eV from $Ga_{0.5}Al_{0.5}As$ values. Photoemission should, therefore, provide an easier test of monolayer quality than optical absorption.

B. $(Ga_{1-x}Al_xAs)_1$-$(Al_{1-x}Ga_xAs)_1$

The success of the VCA in treating $Ga_{1-x}Al_xAs$ justifies its application to monolayer alloy systems based on these constituents. The monolayer heterostructure $(Ga_{1-x}Al_xAs)_1$-$(Al_{1-x}Ga_xAs)_1$ may be produced by random interchange of x cations between the layers of perfect $(GaAs)_1$-$(AlAs)_1$. Calculations on this monolayer system should provide a good model for the effects of diffusion in $(GaAs)_1$-$(AlAs)_1$. If the disorder in existing samples of $(GaAs)_m$-$(AlAs)_n$, $m \approx n \approx 1$, were of a simple diffusional nature, we would expect the calculated $x = 0.3$ results to resemble closely experimental results. The kind of islandlike disorder believed to exist in these materials, however, gives an extra ordering which should produce a band structure between those of $(GaAs)_1$-$(AlAs)_1$ and $(Ga_{0.7}Al_{0.3}As)_1$-$(Al_{0.7}Ga_{0.3}As)_1$. At the moment we are unable to treat islandlike disorder in any more rigorous manner.

The composition dependence of the Γ_5^v, Γ_4^c, and Γ_1^c levels for $(Ga_{1-x}Al_xAs)_1$-$(Al_{1-x}Ga_xAs)_1$ is shown in Fig. 10(a). The zero of energy in this figure has been taken at the pure GaAs valence-band maximum. As can be seen the Γ_4^c level rises especially rapidly as x increases. For $x = 0.30$ the lowest two-band gaps are 1.97 and 2.09 eV. The oscillator strengths are $|\langle\Gamma_5^v|\hat{p}_{x+y}|\Gamma_4^c\rangle|^2 = 0.000\,036$ and $|\langle\Gamma_5^v|\hat{p}_{x+y}|\Gamma_1^c\rangle|^2 = 0.133$. The predicted absorption edge for $(Ga_{0.7}Al_{0.3}As)_1$-$(Ga_{0.3}Al_{0.7}As)_1$ is therefore 2.09 eV. This value is in excellent agreement with the value of ~2.06 eV measured for MBE deposited monolayers.[3] This agreement may be an indication that the disorder in MBE heterostructures actually results from simple diffusion, or

it may be that the islandlike defects in the monolayers are small enough to be adequately modeled by the VCA pseudopotential we used.

In the last column of Table VII we include the energies of those $(Ga_{0.7}Al_{0.3}As)_1$-$(Ga_{0.3}Al_{0.7}As)_1$ levels corresponding to the prominent structures in the $(GaAs)_1(AlAs)_1$ DOS. Again, there are splittings of structures which would be single peaks in $Ga_{0.5}Al_{0.5}As$. However, for this case these splittings are only one-half to one-fourth as great as in $(GaAs)_1$-$(AlAs)_1$. The movement of structures toward higher energies near the top of the DOS is also reduced by diffusion. In keeping with our absorption-edge results, we expect that the DOS for materials with islandlike disorder is between those for $(GaAs)_1(AlAs)_1$ and $(Ga_{0.7}Al_{0.3}As)_1$-$(Al_{0.7}Ga_{0.3}As)_1$ and that splittings should be observable by photoemission.

C. $(GaAs)_1$-$(Ga_{1-x}Al_xAs)_1$

For multilayer heterostructures, $Ga_{1-x}Al_xAs$ with $x \leq 0.3$ is preferred as a barrier between GaAs layers. This is partly because the Ga-rich alloy is a direct band-gap material and partly because the small lattice mismatch is further reduced as $x \to 0$. Since the $(GaAs)_1$-$(Ga_{1-x}Al_xAs)_1$ monolayer can be prepared by the same MBE techniques used to prepare $(GaAs)_1$-$(AlAs)_1$ a preliminary theoretical exploration may be helpful to experimentalists considering which materials should be fabricated. At the moment theoretical explorations are more convenient than experimental.

In Fig. 10(b) we show the composition dependence of two valence-band maxima and five conduction-band minima for this material.

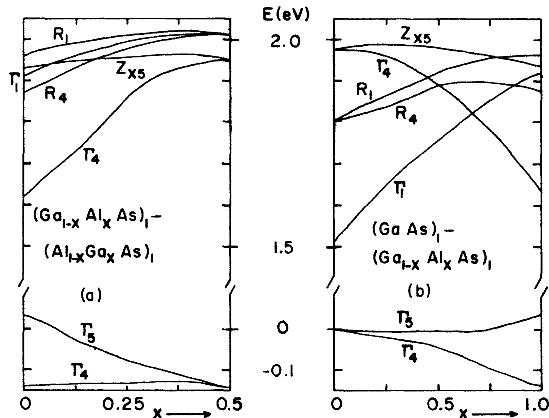

FIG. 10. (a) Composition dependence of the most important energy levels in $(Ga_{1-x}Al_xAs)_1$-$(Al_{1-x}Ga_xAs)_1$. This corresponds to the effects of diffusion x on the $(GaAs)_1$-$(AlAs)_1$ energy levels; (b) composition dependence of the most important eigenvalues of $(GaAs)_1$-$(Ga_{1-x}Al_xAs)_1$.

For $x=0$ (pure GaAs), the Z_{X5} and Γ_4 conduction-band minima are degenerate (the ZB X_1^c). As x increases Z_{X5}^c stays always above Γ_4^c. The Γ_1^c and Γ_4^c levels of $(GaAs)_1(Ga_{1-x}Al_xAs)_1$ lie lower than the Γ_1^c and X_1^c levels of $Ga_{1-0.5x}Al_{0.5x}As$ (the ternary alloy with the same percent of Al) for $0 < x \leq 1$. The change of ordering of the Γ_1^c and Γ_4^c levels at $x = 0.67$ parallels the changed ordering of Γ_1^c and X_1^c in $Ga_{1-x}Al_xAs$ at $x = 0.45$. The crossover in $(GaAs)_1$-$(Ga_{1-x}Al_xAs)_1$ takes place at 33.5% Al, rather than 45% because of the extra ordering in the monolayer material. E_{gc} is also reduced to 1.82 eV as a consequence of the monolayer ordering. Because Γ_1^c is s-like, the Γ_5^v-Γ_1^c optical transition should be observable for all x. Similarly, transition from Γ_5^v to the p-like Γ_4^c should be very weak for all x. Thus, we find that an optical-absorption experiment on $(GaAs)_1$-$(Ga_{1-x}Al_xAs)_1$ should not see the cross-over phenomenon characteristic of $Ga_{1-x}Al_xAs$.

V. CONCLUSIONS AND SUGGESTIONS

GaAs and AlAs are very similar materials. They match well in lattice constant and dielectric constant. Because of these similarities the $(GaAs)_1$-$(AlAs)_1$ structure can be formed by MBE. Several properties of $(GaAs)_1$-$(AlAs)_1$ look very much like superpositions of the properties of GaAs and AlAs: e.g., DOS, $\epsilon_2(\omega)$, and $\rho(\vec{r})$. However, measurements of these properties have not yet been reported. We have performed the first band calculation on this material and, through the relative simplicity of our pseudopotential method, we have been able to calculate all these properties and to show their relation to the properties of the pure materials. For ϵ_2 we find enough extra structure in the monolayer case that we suggest electroreflectance experiments as a method of distinguishing $(GaAs)_1$-$(AlAs)_1$ from GaAs, AlAs, or $Ga_{0.5}Al_{0.5}As$. Our analysis of the valence-band DOS indicates that photoemission should provide a clearer technique than optical absorption for indicating the degree and kind of disorder present in the monolayer materials prepared by MBE.

AlAs and GaAs differ primarily in the positions and energies of their conduction-band minima, GaAs having a direct gap of 1.51 eV and AlAs having an indirect gap of 2.21 eV. As we have shown, the conduction-band minima of $(GaAs)_1$-$(AlAs)_1$ are not at all like those of GaAs, AlAs, or $Ga_{0.5}Al_{0.5}As$. Here the unique ordering of cations which characterizes the monolayer heterostructure has its greatest effect. We have shown that the lowest conduction-band minima (Γ_4, 1.59 eV) is very sensitive to diffusional disorder and very difficult to observe by optical-absorption techniques.

Yet the existence of this state is the most unique property of $(GaAs)_1$-$(AlAs)_1$. As long as it is not detected experimentally, theory and experiment cannot claim to be in agreement. We therefore hope that this work will encourage further experiments such as differential optical absorption, two-photon absorption, and/or photoconductivity. All these techniques should be more sensitive than optical absorption to a weak threshold. A combination of these experiments with photoemission and electroreflectance spectra in the 4–8-eV range would serve both to measure the perfection of MBE monolayer heterostructures and to test the importance of spin-orbit effects neglected in this calculation.

In this paper we have also presented what we believe to be the most successful application to date of the pseudopotential virtual-crystal approximation to a crystalline semiconductor alloy. Our success may be largely attributable to the similarity of the components of the alloy. However, it is known that semiconductor alloy properties depend strongly on the pseudopotentials chosen for the pure materials.[11] We believe that our method of choosing atomic form factors may be combined with composition-dependent dielectric constants to yield accurate VCA band structures for three and four component semiconductor alloys.

We have applied our method of treating substitutional disorder to alloy monolayer heterostructures similar to $(GaAs)_1$-$(AlAs)_1$. Our results for the case of cation self-diffusion indicate that the measured disorder in MBE monolayer heterostructures may be primarily diffusional in nature.

Our results on $(GaAs)_1$-$(Ga_{1-x}Al_xAs)_1$ establish band-gap trends and locate a crossover point at $x_c = 0.67$. For $x < x_c$ the lowest direct band gap should be easily and clearly observable. In the range $0 \le x \le x_c$, E_g can be varied from 1.51 to 1.82 eV.

We hope that our treatments of $(GaAs)_1$-$(AlAs)_1$, GaAs, AlAs, $Ga_{1-x}Al_xAs$, $(Ga_{1-x}Al_xAs)_1$-$(Al_{1-x}Ga_xAs)_1$, and $(GaAs)_1$-$(Ga_{1-x}Al_xAs)_1$ clarify the ways in which electrical and structure properties are related across a series of similar materials.

The method and the form factors used here have also been applied to multilayer heterostructures. Results of these investigations will appear separately.

Note added in proof. In applying this method to multilayer heterostructures we have changed $V_{Ga}(G)$ from the values in Table III to -0.085 Ry and -0.060 Ry for $(aG/2\pi)^2 = 1$ and 2, respectively. This produces a smoother curve when low-G values of $V_{Ga}(G)$ are found by quadratic interpolation. Adjusting the form factors in this way changes individual monolayer eigenvalues by $\lesssim 0.10$ eV and increases the fundamental band gap to 1.77 eV. Peak positions and shapes of curves for DOS, $\epsilon_2(\omega)$, and $\rho(\vec{r})$, however, are not changed. Revised monolayer results, as well as results for multilayer heterostructures will be published in J. Vac. Technol., Aug.-Sept., 1978.

ACKNOWLEDGMENTS

We would like to thank J. P. Van der Ziel for sending us an unpublished preliminary report of his experimental results, A. Majerfield for helpful discussions about the $Ga_{1-x}Al_xAs$ alloy, and Bruce McCombe for a critical reading of this manuscript.

---

*National Research Council-Naval Research Laboratory resident research associate.

[1]L. Esaki and R. Tsu, IBM J. Res. Devel. 14, 61 (1970); and A. Y. Cho, J. Vac. Sci. Technol. 8, 531 (1971).
[2]R. Dingle, W. Wiegmann, and C. H. Henry, Phys. Rev. Lett. 33, 827 (1974).
[3]J. P. Van der Ziel and A. C. Gossard, J. Appl. Phys. 48, 3018 (1977); R. Dingle, J. Vac. Sci. Technol. 14, 1006 (1977).
[4]A. C. Gossard, P. M. Petroff, W. Wiegmann, R. Dingle, and A. Savage, Appl. Phys. Lett. 29, 323 (1976).
[5]P. D. Dernier, D. E. Moncton, D. B. McWhan, A. C. Gossard, and W. Wiegmann, Bull. Am. Phys. Soc. 22, 293 (1977); J. L. Merz, A. S. Barker, Jr., and A. C. Gossard, Appl. Phys. Lett. 31, 117 (1977).
[6]Ed Caruthers and P. J. Lin-Chung, Phys. Rev. Lett. 38, 1543 (1977). The present work uses improved Ga form factors and fits the GaAs conduction-band minima more exactly than was indicated in our preliminary result.
[7]R. H. Parmenter, Phys. Rev. 97, 587 (1955).
[8]John R. Walter and Marvin L. Cohen, Phys. Rev. 183, 763 (1969).
[9]Marvin L. Cohen and T. K. Bergstresser, Phys. Rev. 141, 789 (1966).
[10]E. Hess, I. Topol, K.-R. Schulze, H. Neumann, and K. Unger, Phys. Status Solidi B 55, 187 (1973).
[11]J. A. Van Vechten and T. K. Bergstresser, Phys. Rev. B 1, 3351 (1970).
[12]D. J. Stukel and R. N. Euwema, Phys. Rev. 188, 1173 (1969).
[13]James R. Chelikowsky and Marvin L. Cohen, Phys. Rev. B 14, 556 (1976).
[14]D. D. Sell, S. E. Stokowski, R. Dingle, and J. V. DiLorenzo, Phys. Rev. 7, 4568 (1973).
[15]D. E. Aspnes, C. G. Olson, and D. W. Lynch, Phys. Rev. Lett. 37, 766 (1976).
[16]M. R. Lorenz, R. Chicotka, G. D. Pettit, and P. J. Dean, Solid State Commun. 8, 693 (1970).
[17]C. A. Mead and W. G. Spitzer, Phys. Rev. Lett. 11,

358 (1963).
[18]W. M. Yim, J. Appl. Phys. 42, 2854 (1971).
[19]B. Monemar, Solid State Commun. 8, 2171 (1970).
[20]E. Burstein, H. M. Brodsky, and G. Lucousky, Int. J. Quantum Chem. Symp. 1, 759 (1967).
[21]M. Hass and B. W. Henvis, J. Phys. Chem. Solids 23, 1099 (1962).
[22]J. A. Van Vechten, Phys. Rev. 182, 891 (1969).
[23]Per-Olav Lowdin, J. Chem. Phys. 19, 1396 (1951).
[24]David Brust, Phys. Rev. 134, A1337 (1964); P. J. Lin and J. C. Phillips, *ibid.* 147, 469 (1966).
[25]R. Tsu, A. Koma, and L. Esaki, J. Appl. Phys. 46, 842 (1975).
[26]James R. Chelikowsky and M. Schlüter, Phys. Rev. B 15, 4020 (1977).
[27]P. M. Schneider and W. B. Fowler, Phys. Rev. Lett. 36, 425 (1976).
[28]The labeling of these ZB levels depends on choice of origin. We have taken our origin halfway between an As at $(-\frac{1}{8}a, -\frac{1}{8}a, -\frac{1}{8}a)$ and a Ga at $(\frac{1}{8}a, \frac{1}{8}a, \frac{1}{8}a)$.
[29]John P. Walter and Marvin L. Cohen, Phys. Rev. Lett. 26, 17 (1971); John P. Walter and Marvin L. Cohen, Phys. Rev. B 4, 1877 (1971).
[30]J. C. Phillips, Rev. Mod. Phys. 42, 317 (1970).
[31]W. A. Harrison and S. Ciraci, Phys. Rev. B 10, 1516 (1974). In this theory the charge in the overlap of cation and anion hybrid orbitals, $|h^a\rangle$ and $|h^c\rangle$, is $\{S[(1-\alpha_p^2)^{1/2}-S]\}/(1-S^2)$, $S=0.5$ for all materials, $\alpha_p=0.5$ for GaAs and 0.44 for AlAs.
[32]H. C. Casey, Jr. and M. B. Panish, J. Appl. Phys. 40, 4910 (1969).
[33]R. Dingle, R. A. Logan, and J. R. Arthur, Jr., *Gallium Arsenide and Related Compounds, Edinburgh, 1977*, edited by C. Hilsum (The Institute of Physics, Bristol, 1977), p. 210.
[34]T. Sugeta, A. Majerfeld, A. K. Saxena, and P. N. Robson (unpublished).
[35]W. R. Frensley and H. Kroemer, J. Vac. Sci. Technol. 13, 810 (1976).